

This is a repository copy of *Durability of geopolymer composites reinforced with vegetable fibers: Effects of alkaline activator, matrix dosage, and aging on the composite.*

White Rose Research Online URL for this paper: https://eprints.whiterose.ac.uk/id/eprint/232889/

Version: Accepted Version

Article:

Santana, H.A. orcid.org/0000-0003-1425-9438, Cilla, M.S., Walkley, B. orcid.org/0000-0003-1069-1362 et al. (1 more author) (2025) Durability of geopolymer composites reinforced with vegetable fibers: Effects of alkaline activator, matrix dosage, and aging on the composite. Journal of Building Engineering, 107. 112693. ISSN: 2352-7102

https://doi.org/10.1016/j.jobe.2025.112693

© 2025 The Authors. Except as otherwise noted, this author-accepted version of a journal article published in Journal of Building Engineering is made available via the University of Sheffield Research Publications and Copyright Policy under the terms of the Creative Commons Attribution 4.0 International License (CC-BY 4.0), which permits unrestricted use, distribution and reproduction in any medium, provided the original work is properly cited. To view a copy of this licence, visit http://creativecommons.org/licenses/by/4.0/

Reuse

This article is distributed under the terms of the Creative Commons Attribution (CC BY) licence. This licence allows you to distribute, remix, tweak, and build upon the work, even commercially, as long as you credit the authors for the original work. More information and the full terms of the licence here: https://creativecommons.org/licenses/

Takedown

If you consider content in White Rose Research Online to be in breach of UK law, please notify us by emailing eprints@whiterose.ac.uk including the URL of the record and the reason for the withdrawal request.



DURABILITY OF GEOPOLYMER COMPOSITES REINFORCED WITH VEGETABLE FIBERS: EFFECT OF ALKALINE ACTIVATOR, MATRIX DOSAGE AND COMPOSITE AGING

4 Henrique. A. Santana^{1*}, Marcelo S. Cilla¹, Brant Walkley², Cleber M. R. Dias¹

(1) Department of Materials Science and Technology (DCTM)/ Federal University of Bahia – Rua Aristides Novis 02, Federação. 40210-630, Salvador/BA, Brazil.

(2) Department of Chemical and Biological Engineering, Sir Robert Hadfield Building, The University of Sheffield, Sheffield S1 3JD, United Kingdom.

* almeidahen@gmail.com

10

12

13

14

15

16

17

18

19

20

21

22

23

24

25

26

27

28

29

30

31

1

2

3

5 6

7

8

9

11 ABSTRACT

Vegetable fibers have been identified as a potential solution to the brittle behavior of geopolymers. However, these binders are activated by alkaline solutions, which can degrade the fibers over time and compromise the performance of the composite. This study investigates the impact of different alkaline activators and matrix dosages (low vs. high free ion concentration) on the durability of sisal fiber-reinforced geopolymer composites. Aged composites were evaluated through three-point bending tests and water absorption measurements. The fibers removed from the matrix were evaluated by TG and fibers immersed in the activating solution were analyzed by FTIR. The results show that sisal fibers can enhance the specific energy of the composites. However, mechanical tests revealed a significant reduction—up to 55.82%—in specific energy for composites with high free ion concentration, which were exposed to outdoor conditions for six months. TG analysis highlighted the impact of free alkaline ions on the degradation of noncrystalline components and cellulose in the fibers. FTIR analysis revealed the evolution of fiber degradation following immersion in alkaline solutions. SEM analysis further showed the presence of voids at the fiber-matrix interface in composites with high free ion content. These findings suggest that improper dosing of geopolymer matrices can lead to the degradation of vegetable fibers, regardless of environmental exposure or the type of alkaline activator used. Optimizing the free ion content during matrix formulation can help mitigate, or even prevent, this degradation. A possible degradation mechanism is proposed.

32

33

Keywords: degradation, durability, cellulose, alkaline hydrolysis, sisal fiber.

1. INTRODUCTION

Geopolymer binders can exhibit physical and mechanical properties equivalent to Portland cement while emitting less carbon dioxide (CO₂) throughout their production cycle (Provis et al., 2014; Mohajerani et al., 2019). Currently, there are advanced studies on the production of pastes (Romagnoli et al., 2012), mortars (Latella et al., 2008; Alonso et al., 2017), concretes (Amorim Júnior et al., 2021), precast components (Provis, 2018; Singh et al., 2015), and self-compacting mixes (Santana et al., 2020) based on geopolymer binders.

However, geopolymers are prone to brittle fractures (Alzeer et al., 2013; Yan et al., 2016; Korniejenko et al., 2016), characterized by low energy absorption typical of ceramic materials, which necessitates reinforcement to overcome this limitation. Vegetable fibers (VF) have generated significant interest as potential reinforcements in geopolymer matrices. The advantages of vegetable fibers include their lower density compared to steel and glass fibers, renewable resources, availability in developing countries at a relatively low cost, and their diverse morphological and dimensional variety (Tonoli et al., 2009; Ferreira et al., 2015).

Among the vegetable fibers used as reinforcement in geopolymer matrices are flax fibers (Alzeer et al., 2013; Lazorenko et al., 2020; Assaedi et al., 2017), cotton fibers (Korniejenko et al., 2016; Alomayri et al., 2013), sisal fibers (Correia et al., 2013; Alves et al., 2019; Wongsa, 2020), coconut fibers (Siddharth et al., 2016; Amalia et al., 2017), and pineapple fibers (Correia et al., 2013). Notably, in a recent literature review, Santana et al. (2021) highlighted that the durability of vegetable fibers has not yet been fully investigated, becoming a critical issue due to the fragile physical and chemical stability of these fibers in an alkaline environment.

It is well established that Portland cement-based matrices can degrade vegetable fibers over time through two primary mechanisms that compromise fiber durability: alkaline hydrolysis and mineralization, both of which are associated with the by-products of Portland cement hydration (Toledo Filho et al., 2009; Melo Filho et al., 2013; Wei and Meyer, 2015). In this context, methods for protecting fibers from matrix alkalinity (Kabir et al., 2012; Lima et al., 2014; Ferreira et al., 2017), modifications of matrices to enhance chemical compatibility with lignocellulosic reinforcements (Lima and Toledo Filho, 2008; Pizzol et al., 2014), and the effect of composite aging in natural environments (Dias et al., 2018; Almeida et al., 2013) have been research priorities in recent years. These

studies have contributed to making the application of vegetable fibers in Portland cement-based matrices a reality.

Notably, hydrated calcium silicate (C-S-H) and portlandite (CH) are the primary products formed during Portland cement hydration (Gallucci and Scrivener, 2007). In contrast, geopolymers, which are binders based on aluminosilicate precursors, involve different chemical reactions (Provis and Bernal, 2014). During geopolymerization, the presence of a specific oxide "M" (such as Na₂O or K₂O) leads to the formation of M-A-S-H (M-aluminosilicate hydrate). In systems with calcium-rich precursors, calcium oxide (CaO) can result in the formation of C-A-S-H gel (calcium aluminosilicate hydrate). The extremely alkaline environment of the aqueous phase of the mixtures in their fresh state and the alkalinity of the pore solution of the matrices in their hardened state are the predominant factors of alkali-activated mixtures that can affect the durability of vegetable fibers. Consequently, mechanisms developed to mitigate the degradation of vegetable fibers in Portland cement matrices are unlikely to be effective for geopolymers, since the phases formed in these matrices are not the same.

The production of composites based on vegetable fibers and geopolymer matrices is constrained by the durability of this material. Understanding the behavior of fibers within geopolymer matrices is essential, particularly in light of climatic influences for assessment that can predict long-term performance. To address this, the interaction between vegetable fibers and geopolymer binders was thoroughly studied by evaluating composites produced with different alkaline activators after exposure in a natural laboratory environment and in a natural, outdoor environment.

2. METHODOLOGY

This study evaluates the durability of sisal fiber (Agave Sisalana) used as reinforcement in geopolymer matrices. The geopolymer matrices were prepared with varying levels of aggressiveness. The composites underwent natural aging and laboratory environment exposure.

2.1. Fiber characterization

The sisal vegetable fibers were previously washed in distilled water at 50°C and dried in an oven at 80°C for 48 hours to remove superficially impregnated sugars, thus preserving fiber-matrix adhesion. Fiber samples cut to approximately 1 mm were evaluated by X- ray diffraction, with diffraction spectra obtained over a scanning range (2 θ) from 5° to 50° (**Figure 1a**). The crystallinity index (C_{rl}) was calculated according to **Equation 1**, where I_{cr} is the intensity of the peak of the most crystalline cellulose plane, representing the crystalline region (2 θ between 22° and 23°), and I_A is the peak intensity of the most intense amorphous region for cellulose (2 θ between 18° and 19°).

$$C_{rl} = \frac{I_{cr} - I_{am}}{I_{cr}} \times 100 \tag{Eq. 1}$$

Tensile strength, elongation at break, and Young's modulus were determined through stress-strain curves based on ASTM C1557 (2008). The test was conducted on 15 samples of 50 mm long sisal fibers, using a displacement rate of 2 mm/min on an INSTRON universal testing machine, model 23-10, equipped with a 2 kN load cell. Displacement measurement was performed by tracking the equipment's crosshead movement, as the fibers' short length precluded using an extensometer. Only ruptures occurring near the central section were considered, eliminating the gripping effect on rupture. To calculate the cross-sectional area equivalent to a circle, the equivalent diameters of sisal fibers were determined using an optical microscope, defined as the average of three measurements distributed along the length of each fiber. The stress-strain curve is shown in **Figure 1b**.

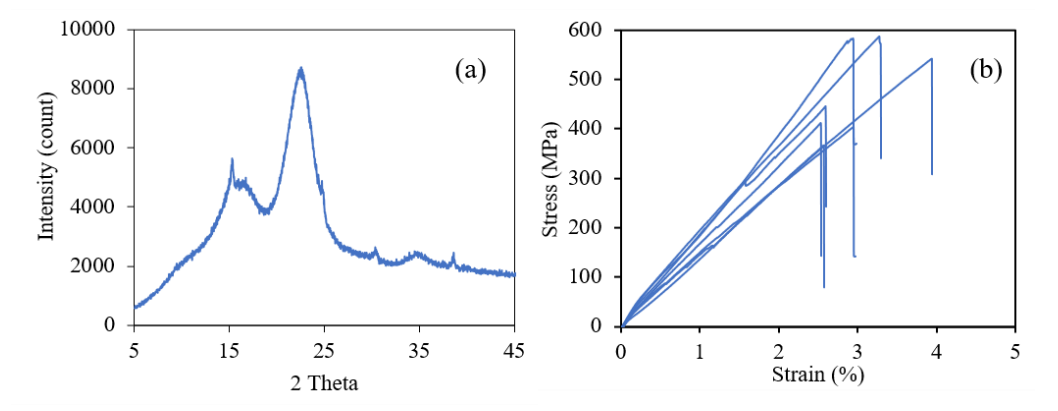


Figure 1 - (a) Diffractogram and (b) stress versus strain curve of sisal fiber.

In determining the water absorption capacity of the fibers $[A_{(\%)}]$, bundles of fibers 30 mm long and approximately 1 g weight were used and dried in an oven at 80°C until a constant mass was achieved, measuring the dry mass (W_1) . Subsequently, the fibers were immersed in water, surface-dried with a damp cloth, and weighed after 48 hours of

immersion, determining the wet mass (W_2) . Water absorption was calculated according to **Equation 2**.

$$A_{(\%)} = \frac{W_2 - W_1}{W_1} \times 100$$
 (Eq. 2)

The fiber density (ρ) was determined using a helium gas pycnometer (AccuPyc II 1340 Micromeritics). **Table 1** provides a complete characterization of the sisal fiber.

Table 1 - Physical, mechanical, and mineralogical characterization of sisal fiber.

$rac{\mathcal{C}_{rl}}{(\%)}$	Stress (MPa)	Strain (%)	Young Modulus (GPa)	A (%)	ρ (g/cm²)
69.99	466.86 ± 95.66	2.81 ± 0.29	16.55 ± 2.32	189.19	1.59 ± 0.04

The characteristics determined for sisal fiber show values close to those observed in the literature (Wei and Meyer, 2016; Yan et al., 2016). It should be noted that, as it is a natural material, its characteristics cannot be fully controlled during harvesting and processing, leading to the large expected variation in physical and mechanical properties.

2.2. Dosage and characterization of the matrix

To assess the influence of dosage efficiency of alkali-activated matrices on fiber durability, prediction models for properties were employed, as established in a previous study (Santana et al., 2023). These models were determined using the statistical mixture design (SMD), employing Design-Expert® software, i-Optimal Custom Designs tool, and Best algorithm. Consequently, four formulations of geopolymers were established based on boundary conditions:

- i) GNa_{min} Geopolymeric matrix activated with sodium silicate solution, optimized to minimize the concentration of free alkali ions in the pore solution.;
- ii) GNa_{max} Geopolymeric matrix activated with sodium silicate solution, optimized to maximize the concentration of free alkali ions in the pore solution;
- iii) GK_{min} Geopolymeric matrix activated with potassium silicate solution, optimized to minimize the concentration of free alkali ions in the pore solution.
- iv) GK_{max} Geopolymeric matrix activated with potassium silicate solution, optimized
 to maximize the concentration of free alkali ions in the pore solution.

The Metacaulim HP Ultra (MK) from *Metacaulim do Brasil*, and term-treated asbestos cement waste (ACW_T) were used as precursors. The ACW_T was carefully treated according to the methodology detailed in Carneiro et al. (2021). The activating solutions were produced with densified silica fume supplied by *Companhia de Ferro Ligas da Bahia*, sodium hydroxide (NaOH), and potassium hydroxide (KOH), with 98% purity. **Table 2** presents the specific gravity of metakaolin, silica fume, and ACW_T, determined by helium gas pycnometer (AccuPyc II 1340 Micromeritics), specific surface area determined by BET method on a Gemini VII Micromeritics Pycnometer, and chemical composition obtained by X-ray fluorescence using a Bruker S2 Ranger spectrometer. The precursor materials' average particle diameter (Da) was determined by dry laser diffraction (S3500 Microtrac).

Table 2 - Chemical composition and physical properties of materials.

Materials	Metakaolin	ACW _T	Silica fume
Physical properties			
Skeletal density (g/cm ³)	2.80	2.95	2.32
BET specific surface area (m²/g)	30.52	6.68	15.15
Da	20.29	18.80	-
Chemical composition (%)			
SiO_2	44.88	18.20	81.75
Al_2O_3	42.86	4.06	1.41
Fe_2O_3	4.82	2.35	4.90
K ₂ O	0.72	0.34	1.82
SO_3	0.13	1.66	0.51
MgO	0.67	7.27	1.34
MnO	0.11	-	0.13
CaO	-	48.69	0.29
Others	1.41	1.13	3.46
Loss on ignition (1000 °C)	4.23	16.30	4.40

Metakaolin is predominantly composed of alumina and silica, essential for M-A-S-H production. In contrast, ACW_T is rich in calcium and can promote the formation of C-A-S-H, C-S-H, and portlandite. The use of these two precursors with different chemical

compositions was motivated by the need to assess the durability of vegetable fibers with various compounds.

Sodium and potassium silicate solutions were prepared in the laboratory to evaluate the influence of alkaline base (NaOH or KOH) on the durability of vegetable fibers. Liquid sodium silicate (LSS) was synthesized with 52% deionized water, 27% silica fume (SF), and 21% sodium hydroxide (NaOH) by mass (molar ratio SiO₂/Na₂O of 1.33). Liquid potassium silicate (LKS) was produced with 49% deionized water, 27% SF, and 24% potassium hydroxide (KOH) by mass (molar ratio SiO₂/K₂O of 1.16). The silicate solutions were prepared with different compositions because NaOH showed greater efficiency in precursor material decomposition reactions in preliminary laboratory tests. The activating solution materials were manually mixed, the container was sealed with plastic film, and the solution was used after cooling to room temperature.

The compressive strength (C_S) of the pastes was determined on three cubic specimens measuring 40 mm per side per formulation after 28 days of curing in an environment with a temperature of (25 ± 2) °C and relative humidity of (65 ± 5) %. Testing was conducted using a servo-hydraulic press with a capacity of 1200 kN at a loading rate of 500 N/s. The density of the pastes (ρ) was measured using a helium gas pycnometer (AccuPyc II 1340 Micromeritics).

Control of free alkali ions in the pore solution of the matrix was indirectly conducted by measuring the electrical conductivity of the residual solution (σ) obtained after samples were immersed in distilled and deionized water. The chemical composition of the residual solution was determined using a flame atomic absorption spectrometer (Varian, 220 FS). The mass fractions and characteristics of the formulations are presented in **Table 3**.

Table 3 - Formulations of alkali-activated matrices used in the exposure test.

Formulation	Weight fraction			Properties			Chemical composition				
	MK	ACW_T	Ativador	Cs (MPa)	ρ (g/cm²)	σ (mS/cm)	Ca (mg/L)	Mg (mg/L)	Na (mg/L)	K (mg/L)	pН
GNa _{min}	0.474	0.013	0.513	60.35 ± 1.81	2.35 ± 0.006	7.88	< 2	< 2	301	106	10.85
GNa _{max}	0.286	0.127	0.586	40.42 ± 0.55	2.14 ± 0.003	28.60	< 2	< 2	2753	43	10.10
$\mathbf{G}\mathbf{K}_{\mathbf{min}}$	0.490	0.000	0.510	57.36 ± 2.89	2.44 ± 0.017	7.58	< 2	< 2	222	107	10.76
$\mathbf{G}\mathbf{K}_{max}$	0.252	0.148	0.600	33.55 ± 0.03	2.25 ± 0.017	28.50	< 2	< 2	243	8802	10.04

2.3. Production and aging of the composites

For the production of the composites, fibers were cut to a length of 25 mm, established based on the critical length (defined as the minimum length for stress accumulation equal to the breaking stress), determined in preliminary laboratory tests. A fiber content of 2.5% by mass of the precursor was used, a value determined based on the maximum proportion that did not affect the workability of the mixture.

The four pre-dosed pastes were produced in a 5 L planetary mixer. Metakaolin and ACW_T were mixed for 30 seconds, followed by the addition of the activating solution for another 30 seconds, and mixed for an additional 30 seconds. Subsequently, the mixer was turned off for 30 seconds to scrape the sides of the bowl and the mixer paddle. After this period, the mixer was turned on again, and sisal fibers were added to the mixture, which was kept running for another 30 seconds to homogenize the fibers with the paste. The process was conducted at a low speed $(62.5 \pm 5 \text{ rpm})$. The composites were molded into prismatic forms with internal dimensions of 230 mm x 50 mm x 10 mm, ensuring homogeneous and dispersed fiber distribution. The molds were kept in a laboratory environment at (25 ± 2) °C and (65 ± 5) % relative humidity for 24 hours, followed by demolding and placement in the exposure environment (**Fig. 2**).

Three composites per group were evaluated after exposure in a laboratory environment for 28 days (28Lab series), laboratory aging up to 120 days (120Lab series), and natural exposure aging up to 120 days (120Nat series). All groups remained in the laboratory for 28 days to ensure that all alkali-activation reactions had occurred before exposure.

The samples were exposed on the terrace of the School of Engineering at the Federal University of Bahia, Brazil, located at latitude 12° 59 '58.30 " S and longitude 38° 30' 37.07" W, according to the WGS 84 geodetic reference system. Based on the works of Dias (2005), and Almeida et al. (2013), the specimens were placed in galvanized steel supports facing true north, with a 45° inclination relative to the horizontal plane.

The exposure period chosen involved daily precipitation and significant thermal fluctuations (see Figure 2), exposing the composites to repeated wetting and drying cycles. Samples designated for natural exposure were kept in the laboratory for 72 hours under the same conditions as the other samples, ensuring uniform moisture content across all specimens before testing.

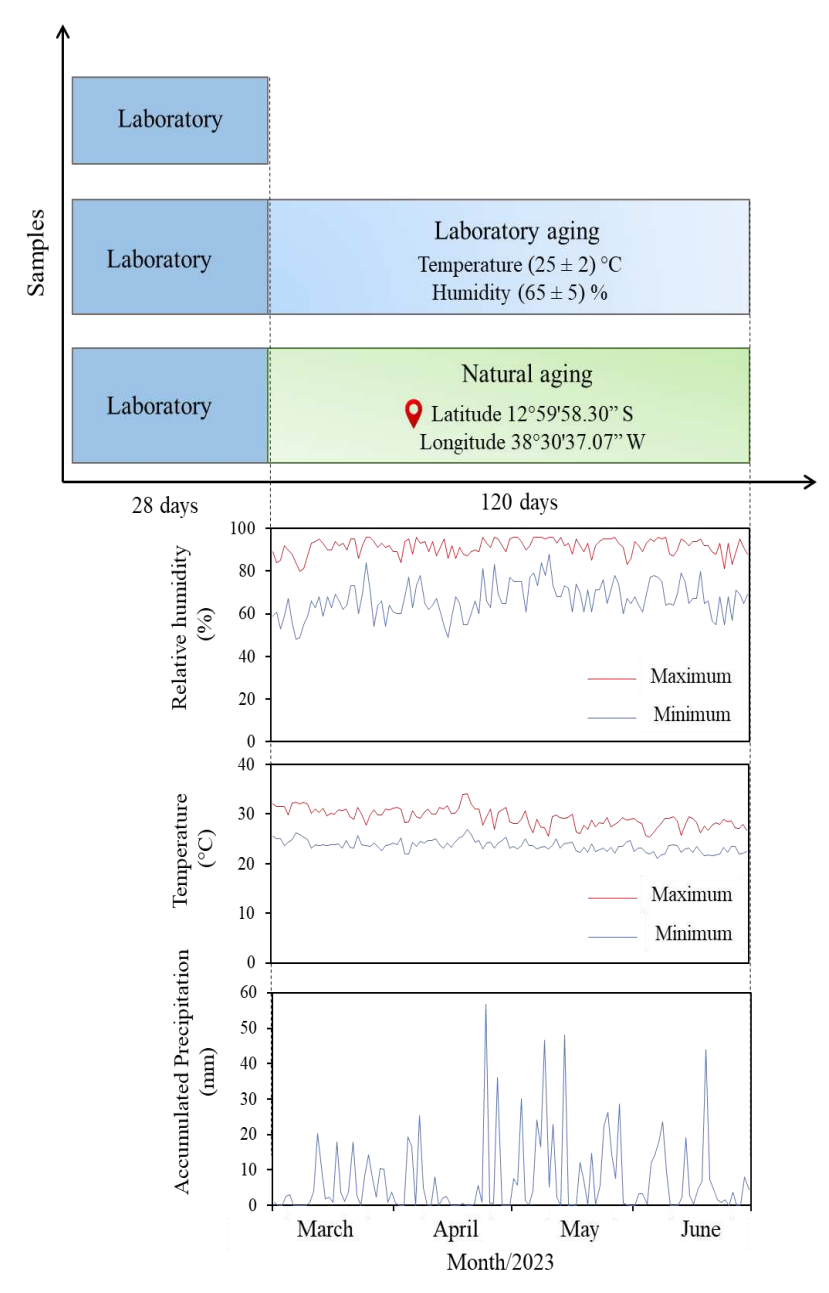


Figure 2 - Exposure conditions for the three groups of composites under study.

2.4. Chemical analysis of fibers by FTIR

To evaluate the chemical modifications of the fibers when exposed to the activating solutions, the reference fibers (as received) were divided into two groups: one immersed in the SSL solution and the other in the SSK solution. Samples were taken after 10 minutes, 1, 6, 24, and 160 hours of immersion and analyzed by Fourier Transform Infrared Spectroscopy (FTIR). Fiber samples were cut to approximately 1 mm in length, and 2 grams of the samples were analyzed using Attenuated Total Reflectance (ATR). Data were collected in the 400 to 4000 cm⁻¹ wavenumber range using a Thermo Fisher

Nicolet iS5 FTIR spectrometer equipped with a Specac Golden Gate Single Reflection Diamond ATR System. Each spectrum represents the average of 64 scans with a spectral resolution of 2 cm⁻¹. The spectra were normalized using the band centered at 3750 cm⁻¹ as a reference, which was not affected by the immersion of the fibers in the alkaline solution.

2.5. Physical and mechanical evaluations of composites

The capacity of water absorption (C_W) of the composites after exposure to different environments was determined by measuring the dry mass (W_1) and the water-saturated mass (W_2) of three specimens per formulation and calculated using **Equation 3**.

$$C_W = \frac{W_2 - W_1}{W_1} \times 100$$
 (Eq. 3)

The dry mass of the specimens was obtained after drying in an oven for 72 hours at a temperature of 50 ± 2 °C, and the saturated mass was determined after 48 hours of immersion in water.

To determine mechanical properties, a 3-point bending test was conducted with a span between supports of 170 mm, using a displacement rate of 0.5 mm/min on an INSTRON universal testing machine, model 23-10, equipped with a load cell capacity of 2 kN. The limit of proportionality (LOP) of the composites was determined from the load (N) versus deflection (mm) curve (Eq. 4).

$$LOP = \frac{F_f L}{wh^2}$$
 (Eq. 4)

Where F_f is the load at the point on the load-deflection curve where behavior becomes nonlinear (N), L is the distance between the supports (170 mm), w is the width, and b is the height of the cross-sectional area of the sample (mm).

The absorbed energy during the test was determined by integrating the load versus deflection curve. The specific energy (SE) was determined at different deflection levels by the ratio of absorbed energy to the cross-sectional area of the samples:

- 269 (i) $SE_{(0-1)}$ level between 0 and 1 mm of deflection, referring to the region before any cracking occurs, where the transfer of elastic stress is the dominant mechanism and
- 271 longitudinal displacements of the fiber and matrix at the interface are geometrically
- 272 compatible;
- 273 (ii) SE₍₁₋₉₎ level between 1 and 9 mm of deflection, referring to the region characterized
- by the appearance of multiple cracks supported by fiber anchoring. Subsequently, existing
- 275 cracks begin to open, supported by the fiber length (25 mm). This widening is intensified
- at the central crack in the direction of the flexural load application;
- 277 (iii) SE₍₁₀₋₂₀₎ level between 10 and 20 mm, referring to the region where the bonds
- between fibers and the matrix are broken, resulting in a decrease in load with an increase
- in deflection of the composites.

281

2.6. Thermogravimetric analysis

- Thermogravimetric analyses of sisal fibers removed from the composites were
- conducted using a Perkin Elmer TGA 4000 thermobalance under a nitrogen atmosphere,
- with a heating rate of 10 °C/min from 30°C to 900°C. Approximately 7.5 mg of fibers
- were used for each test.

286

287

2.7. Microstructural analysis

- The microstructure of fractured sections of the composites was investigated using
- a Hitachi TM3030 scanning electron microscope. The microscope operated under an
- acceleration voltage of 15 kV. A thin carbon layer was applied to the samples to make
- 291 them conductive and suitable for analysis. Additionally, the polished section was
- analyzed after embedding in a polymer resin, facilitating observation of the interface zone
- between the matrix and the fiber.

294

295

296

3. RESULTS

3.1. Chemical analysis of fibers by FTIR

- Figure 3 presents the spectra of the fibers after immersion for 10 minutes, 1, 6,
- 298 24, and 160 hours in the activating solutions LSS and LKS. The five main bands of the
- spectra for the fibers subjected to sodium- and potassium-based activating solutions were
- 300 highlighted.

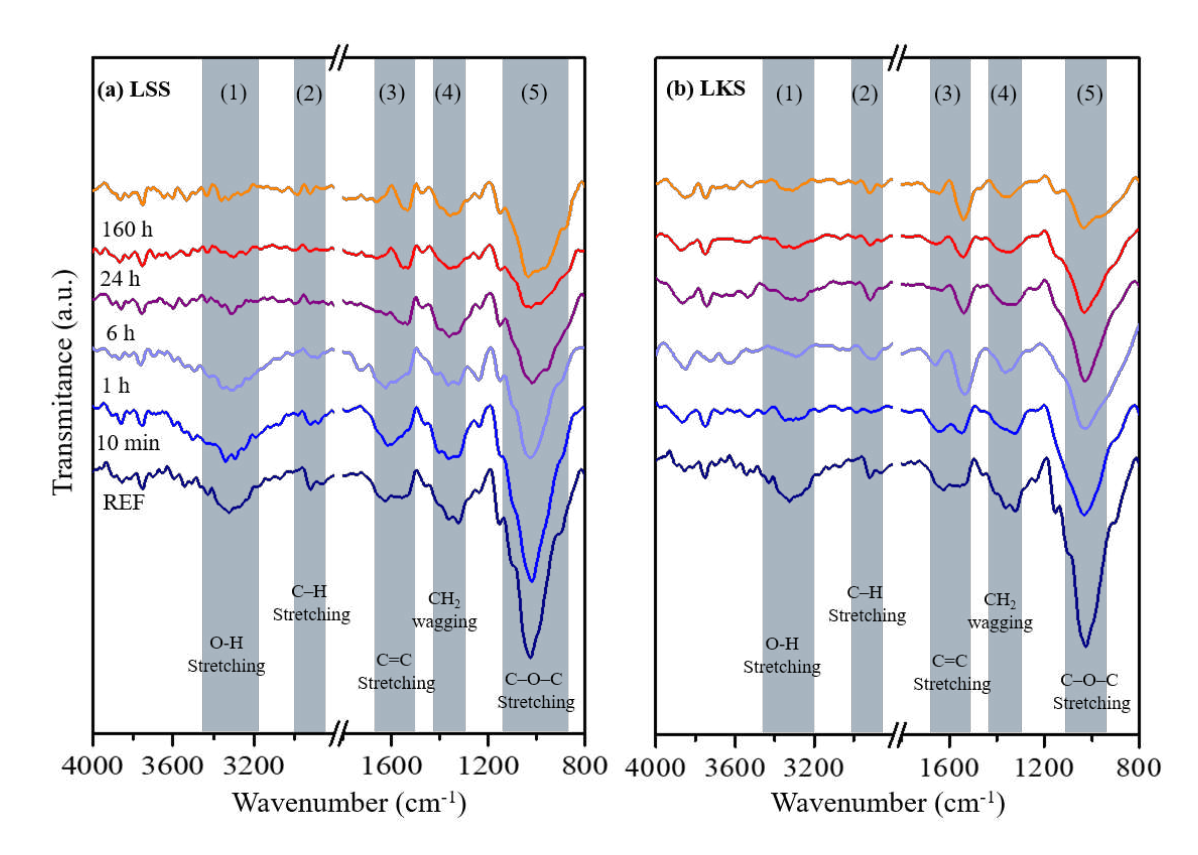


Figure 3 – FTIR spectra for fibers immersed in solutions of (a) liquid sodium silicate (LSS) and (b) liquid potassium silicate (LKS), analyzed after 10 minutes, 1, 6, 24, and 160 hours.

The first band (1), centered at the wavenumber of 3300 cm⁻¹, is associated with the intramolecular and intermolecular OH stretching of the lignin, cellulose, and hemicellulose molecules (Yang et al., 2007; Oudiani et al., 2017; Salim et al., 2021). The second band, located at the wavenumber of 2900 cm⁻¹, corresponds to the C–H stretching also in the cellulose, hemicellulose, and lignin molecules (Yang et al., 2007; Salim et al., 2021). The third band (3), located around the wavenumber of 1550 cm⁻¹, is associated with the C=C stretching of the aromatic ring of lignin (Mohan et al., 2012; Kamarudin et al., 2020). The fourth band, at 1350 cm⁻¹, corresponds to CH₂ wagging in cellulose (Oudiani et al., 2017; Javier-Astete et al., 2021; Salim et al., 2021). The last band, centered at 1000 cm⁻¹, corresponds to the C–O–C stretching of cellulose and hemicellulose (Yang et al., 2007; Javier-Astete et al., 2021). Additionally, the band between 1650 and 1630 cm⁻¹, overlapping with the region indicating C=C stretching of the aromatic ring in lignin, is attributed to absorbed water in cellulose (Álvarez et al., 2006).

The first two bands, related to hydrogen bonding in hemicellulose, cellulose, and lignin, show a reduction in intensity with longer immersion periods. Hemicellulose and lignin are amorphous components that are easily degraded in alkaline solution, while cellulose is protected by the first two, making it the last to be compromised (Wei and Meyer, 2015). The third band, related to the stretching of the aromatic ring of lignin, did not show as significant changes as the first bands, indicating that the molecules composing lignin were not completely compromised by the alkaline solutions, a result that is more evident in fibers exposed to LKS. The bands in regions 4 and 5, related to chemical modifications in the cellulose, also showed slight reductions in intensity for fibers immersed in both solutions. Possibly, after the initial degradation of lignin and hemicellulose, the bonds that hold the cellulose microfibrils together may have been compromised, but the microfibrils remained stable, even after 160 hours of immersion.

It is worth noting that immersing the fibers in alkaline solutions is an extreme condition, and in alkali-activated matrices, a large portion of the alkaline ions present in the solution will have reacted with the matrix and will no longer be available to promote this mechanism. On the other hand, the alkalinity at the time of mixing is analogous to the alkalinity of the activating solution. According to Santana et al. (2021), the pH of the metakaolin-based geopolymeric mixture activated by sodium silicate (silica fume, sodium hydroxide, and water) effectively decreases after about one hour. Thus, the decomposition of the fiber components, as indicated by the spectra obtained at 10 minutes and 1 hour, is expected to occur. Minimizing free ions in the solution within the matrix pores is one of the major challenges in studies of this class of binders, as it not only ensures the durability of materials used as reinforcement but also reduces the manifestation of efflorescence on the material surfaces.

3.2. Composites water absorption capacity

Figure 4 shows the water absorption capacity of the composites after exposure to the three proposed environmental conditions.

It is known that composites produced with cementitious matrices and vegetable fibers exhibit higher water absorption than the matrix (PAGE et al., 2019), justified by the higher water absorption capacity of the fibers. The increased water absorption capacity indicates the increment in connected pores within the matrix, which in composites can be caused by the decomposition and leaching of fibers in the alkaline

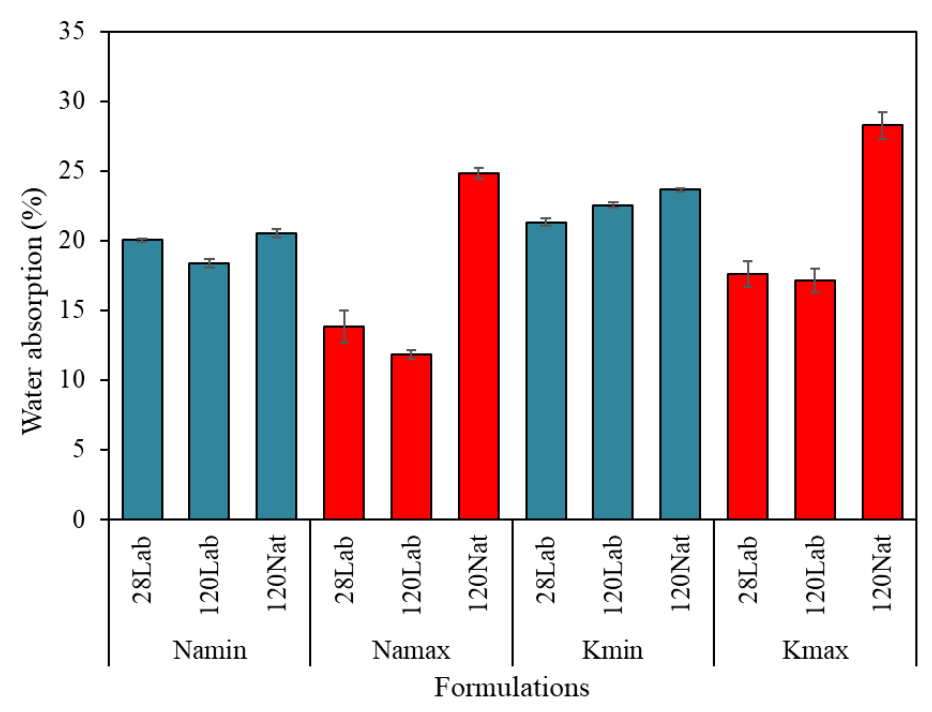


Figure 4 – Water absorption capacity of the evaluated composites.

It is noted that composites produced with matrices of higher alkaline aggressiveness (Na_{max} and k_{max}) showed lower water absorption capacity after exposure in the laboratory environment (28Lab and 120Lab) than Na_{min} and K_{min} composites. This behavior can be attributed to the lower proportion of activating solution in the matrices of Na_{min} and K_{min} composites and, consequently, the higher viscosity of the paste, favoring the formation of voids during mixing with the fibers.

In contrast, for the Na_{max} and k_{max} composites after exposure to the natural environment (120Nat), the influence of weather conditions and weathering on the increase in water absorption capacity is evident. Increases of 79.6% and 70.6% were observed for Na_{max} and k_{max} , respectively, compared to the same composite groups that remained in the laboratory for 28 days, and increases of 109.5% and 60.1% compared to composites that remained in the laboratory for 120 days. According to Juarez et al. (2007), variations in humidity and temperature can induce cracks and microcracks due to drying shrinkage of the matrix. These cracks facilitate moisture flow from the external environment, leaching products weakly bonded to the matrix structure. Moreover,

moisture transport within the matrix can cause the dissolution of free alkaline ions, increasing the alkalinity of the water solution in contact with the vegetable fibers.

Kani et al. (2012) highlighted that potassium-based geopolymers are less susceptible to efflorescence formation due to the strong bond of potassium within the geopolymers' structure, aligning with the observed result where composites produced with sodium-based matrix showed higher water absorption capacity. Indeed, a significant portion of the sample mass may have decreased after sodium leaching due to weathering actions.

3.3. Mechanical evaluation

Figure 5 shows the load versus deflection curves of the composites after exposure in the laboratory environment for 28 days (28Lab) and 120 days (120Lab) and after exposure in the natural environment for 120 days (120Nat).

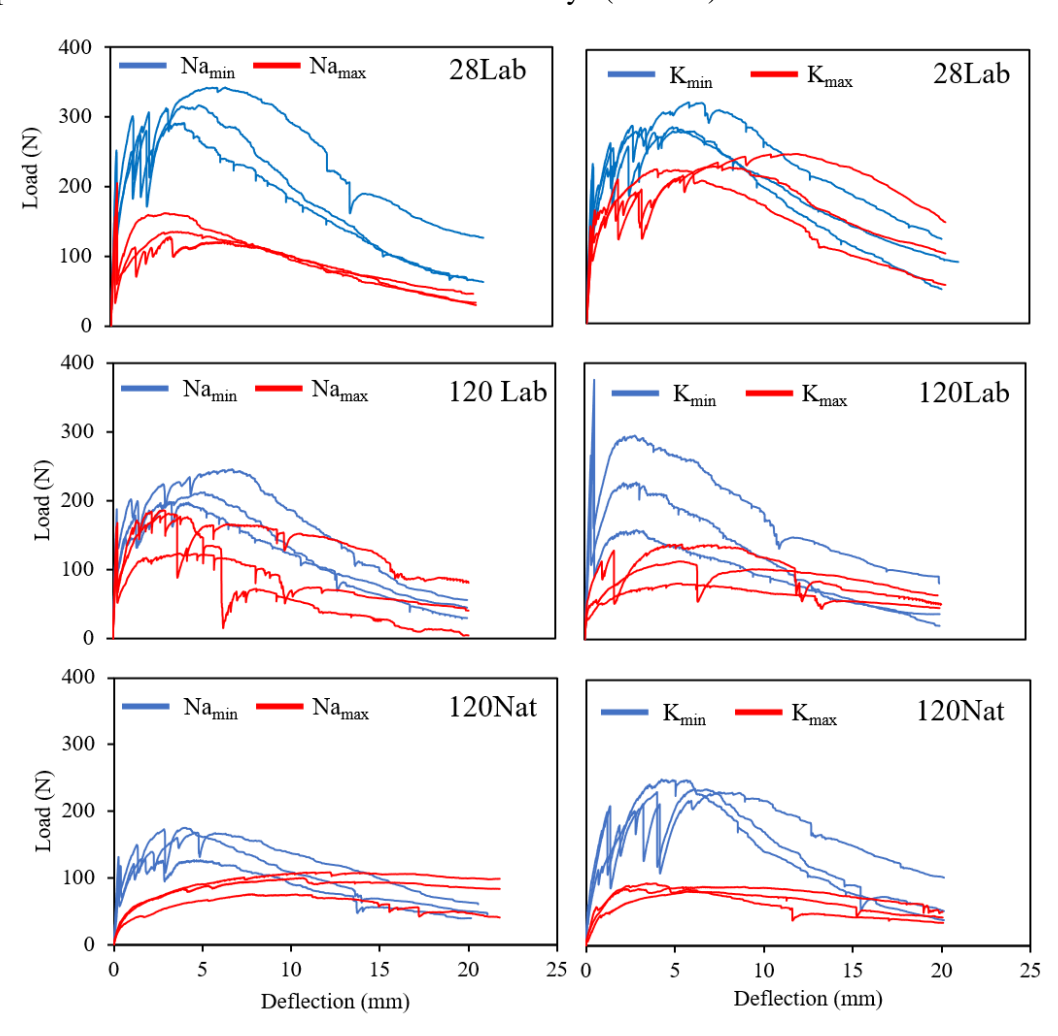


Figure 5 – Load versus deflection behavior for the composites exposed in the three different exposure conditions (28Lab, 120Lab and 120Nat).

The geopolymeric composites reinforced with vegetable fibers exhibited the characteristic behavior of a Portland cement-based composite reinforced with vegetable fiber, as presented by Melo Filho et al. (2023). The curves obtained in the three-point bending test made it possible to determine the limit of proportionality (LOP) and the specific energy (SE) of the evaluated samples.

3.3.1 Limit of proportionality (LOP)

Figure 6 presents the LOP values obtained from the load versus deflection curves of the composites, highlighting the influence of both the exposure environment and the matrices on the observed values.

When analyzing the LOP values, which refers to the stress where the first crack occurred at the end of the elastic-linear phase in the stress versus deflection curve, it is observed that the Na_{max} and K_{max} composites exhibited inferior performance compared to the Na_{min} and K_{min} composites, regardless of the exposure environment. The LOP is a property influenced by the stiffness of the matrix, and the matrices of Na_{max} and K_{max} composites were previously characterized with lower compressive strength and higher porosity. Furthermore, the high alkalinity of these matrices can induce fiber degradation processes, further contributing to the lower LOP values observed.

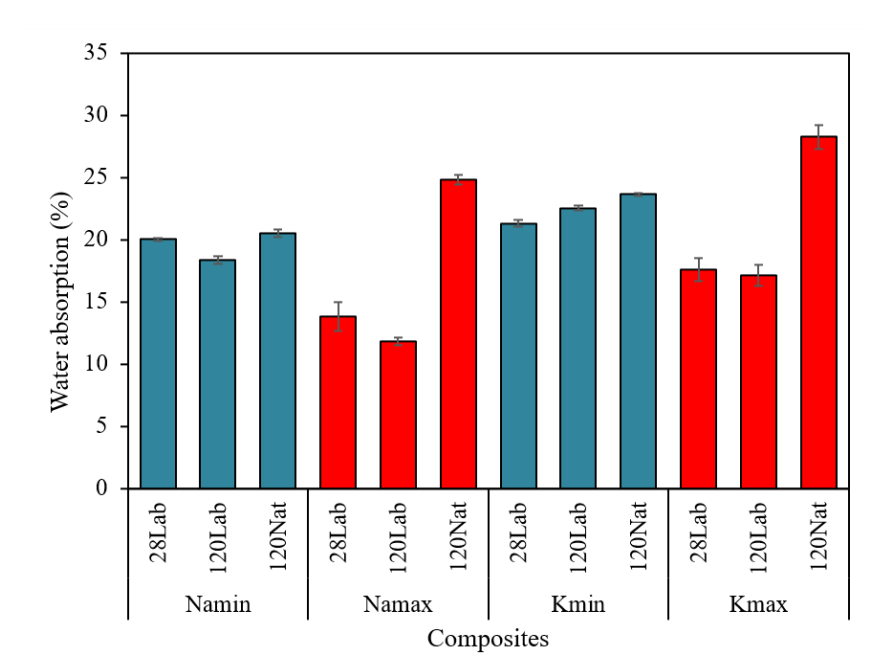


Figure 6 – Limit of proportionality obtained from the load versus deflection curve.

The Na_{max} and K_{max} composites exposed to the natural environment did not show well-defined first crack peaks. In Fig. 2, it can be observed that the composites were subjected to intense daily cycles of wetting and drying due to recurring precipitation during the exposure period. As discussed by Juarez et al. (2007), variations in humidity and temperature can lead to cracks and microcracks due to dimensional changes in the composite, meaning the matrices were already cracked at the beginning of the test, and the fibers temporarily bear the load applied to the composite. During the setting of cementitious pastes, vegetable fibers can absorb water and contribute to the shrinkage of the matrix, consequently compromising the adhesion between the phases of the composite (Ferreira et al., 2020), a predominant factor for Na_{max} and K_{max}, which have a higher proportion of liquid in their compositions. Additionally, Ballesteros et al. (2019) emphasize that vegetable fibers exhibit hydrophilic performance, which creates incompatibility and loss of adhesion at the interface between the fiber and the matrix, potentially exacerbated by the higher porosity of these composites.

It is noted that for sodium-based matrices, the environment and exposure time were effective variables affecting the LOP of the composites, with the following intensity order observed: 28Lab > 120Lab > 120Nat. This behavior can also be explained by the weakening of the matrix caused by drying shrinkage over time, described in the literature as a common issue in geopolymeric matrices (Amorim Junior et al., 2021; Zhang et al., 2022), which climatic variations can exacerbate. Additionally, there may be weakening of the vegetable fiber through alkaline hydrolysis (Wei and Meyer, 2015), enhanced by moisture in the natural environment and dimensional variations in the fibers (Melo Filho et al., 2013), leading to internal stresses in the matrix or discontinuities after degradation.

Differing the LOP behavior observed for composites produced with sodium-based matrices, it is noted that K_{min} showed a superior LOP result after 120 days of exposure in the laboratory environment compared to K_{min} after 28 days under the same laboratory conditions. It was observed that this group of composites exhibited well-defined first crack load peaks, with a single crack opening in the center of the composite and a sudden transfer of load from the matrix to the fibers in this region. Before cracking, the bond between the fiber and the matrix is sustained by chemical adhesion and friction, which may have contributed to the load peak. Subsequently, the high stress transferred abruptly from the matrix to the fiber may have exceeded the shear stress between these two materials, causing a sudden reduction in the load that was subsequently recovered, indicating that the fibers still can support loads, even after 120 days in the matrix.

In comparison between alkaline activators, it is noticeable that only in 28Lab are the LOP values for sodium-based matrices higher than those for potassium-based matrices. One hypothesis for the change in this behavior for 120Lab and 120Nat lies in the increased release of ions in the sodium-based matrices, which may have compromised the adhesion between phases, meaning the shear stress between the fiber and the matrix was reduced over time due to potential reactions between free sodium ions and the cellulose structure.

3.3.2 Specific energy (SE)

Specific Energy (SE) was determined through the area under the load versus deflection curve obtained in the 3-point bending test, analyzed at three deflection levels (**Figure 7**).

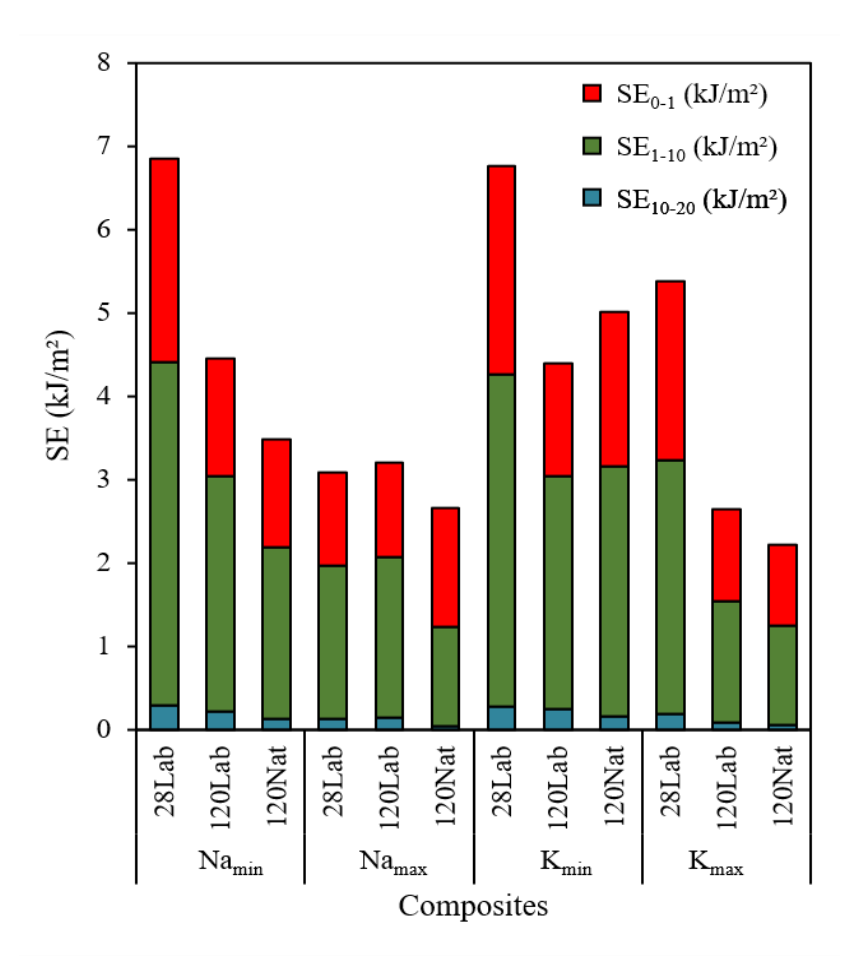


Figure 7 – Specific energy determined for the groups of composites evaluated.

To understand the behavior of the composites, it is necessary to consider that fibers are more effective in the post-cracking zone, acting as reinforcements in the cracked regions. In these areas, fibers can cause two effects on the matrix (Bentur and Mindess, 2006): i) deflection hardening, characterized by an increase in the composite's strength to values greater than the matrix's strength, achieved through stress transfer to the fibers; ii) deflection softening, increasing the toughness of the composite by absorbing energy through fiber pull-out, even with a decreasing load versus deflection curve after cracking.

These behaviors are associated with a specific critical volume of fibers in the composite, where when the fiber volume equals or exceeds this critical volume, deflection hardening behavior is expected, as predominantly seen in the results depicted in Figure 6. In this context, in addition to fiber behavior, the fiber volume also governs the specific energy of the composite. The fiber volume used in this study (2.5%) is higher than typical values observed in the literature for Portland cement-based matrices. The K_{min} samples that exhibited deflection softening behavior in 120Lab were likely influenced by increased load on the matrix and abrupt transfer to the fibers after the first crack.

Regarding specific energy, it is noted that the first deflection level (SE_{0-1}), the region predominantly contributed by the matrix, shows more effective values for the Na_{min} and K_{min} composites produced with matrices optimized with higher compressive strength, lower porosities, and minimized free alkalis, aligning with the results observed for the LOP.

The specific energy of the second level (SE₁₋₁₀) represents the fiber's ability to absorb energy after the matrix rupture. It serves as an indicator of the bond strength between the fiber and the matrix, as well as the degradation of the fiber due to the action of free alkalis in the pore solution. As expected, the SE₁₋₁₀ values were higher for the Na_{min} and K_{min} composites at 28 days. It is noteworthy that the SE₁₋₁₀ value for K_{min} at 120Nat (2.99 kJ/m²) was 31.7% higher than the value obtained for the Na_{min} composite under the same conditions, demonstrating that the K_{min} composite exhibits superior performance even under the most critical environmental condition (120Nat). It is also noted that, even after 120 days of exposure to the natural environment, the Kmin composite exhibits between 3 and 5 cracks in the matrix (indicated by the abrupt reduction in load in the three-point bending test curves). After all cracks have occurred, the composite recovers its load-bearing capacity, achieving values higher than those at the first crack.

Another crucial factor influencing the specific energy of the composite is the critical length of the fibers. According to Bentur and Mindess (2006), when the fiber

length is shorter than the critical length, there is not enough length to generate a stress equal to the fiber's strength, meaning the fiber is not entirely effective. However, if the fiber length exceeds the critical length, the stress along the fiber will reach its tensile strength, thus utilizing most of the fiber's potential.

According to the load versus deflection curves of the evaluated composites, the critical length can vary depending on the properties of the matrix and the exposure environment. In this study, the critical length was determined for the Na_{min} matrix through pull-out tests and adopted for the other composites. It is sufficient to observe the behavior of the composite produced with the same Na_{min} matrix after 120Nat, where a longer fiber length is likely required to compensate for the loss of specific energy caused by the loss of adhesion between the composite phases.

Finally, it is noteworthy that for the Na_{max} and K_{max} composites, after 120 days in the natural environment, the specific energy values for the last deflection level (SE_{10-20}) are close to SE_{1-10} . In fact, the stress-strain curve for these composites shows a constant behavior without significant variations in the supported load, indicating that the fibers are easily pulled out from the matrix and the bond strength is ineffective. Adhesive strength is compromised when fibers are gradually degraded, affecting the bond with the matrix and forming voids at the interface zone.

3.4. TG Analysis

Figure 9, Figure 10, and **Figure 11** show the results of thermogravimetric analysis for the fibers extracted from the matrix after aging in different environments. The thermal decomposition of sisal fiber components occurs gradually through the vaporization of absorbed water (40 and 115 °C), decomposition of hemicellulose and glycosidic bonds of cellulose (220 to 315 °C), cellulose decomposition (315 to 400 °C), and decomposition of lignin, which has a complex structure of aromatic rings, occurring over a wide temperature range (Fiore et al., 2016; Zhou et al., 2014).

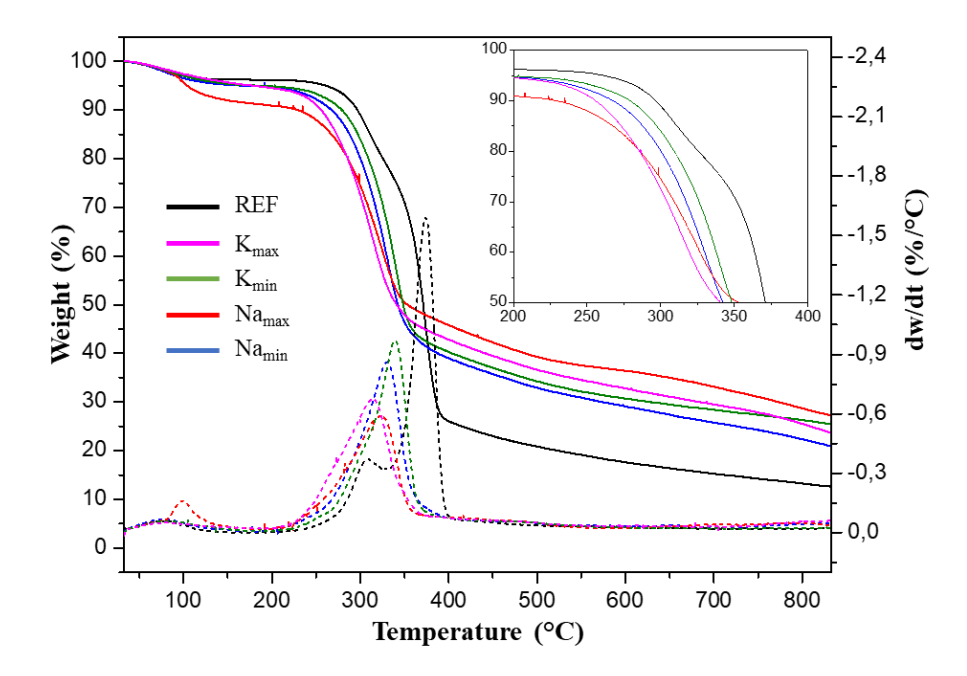


Figure 9 – Thermogravimetric analysis for fibers extracted from the matrix after exposure in 28Lab.

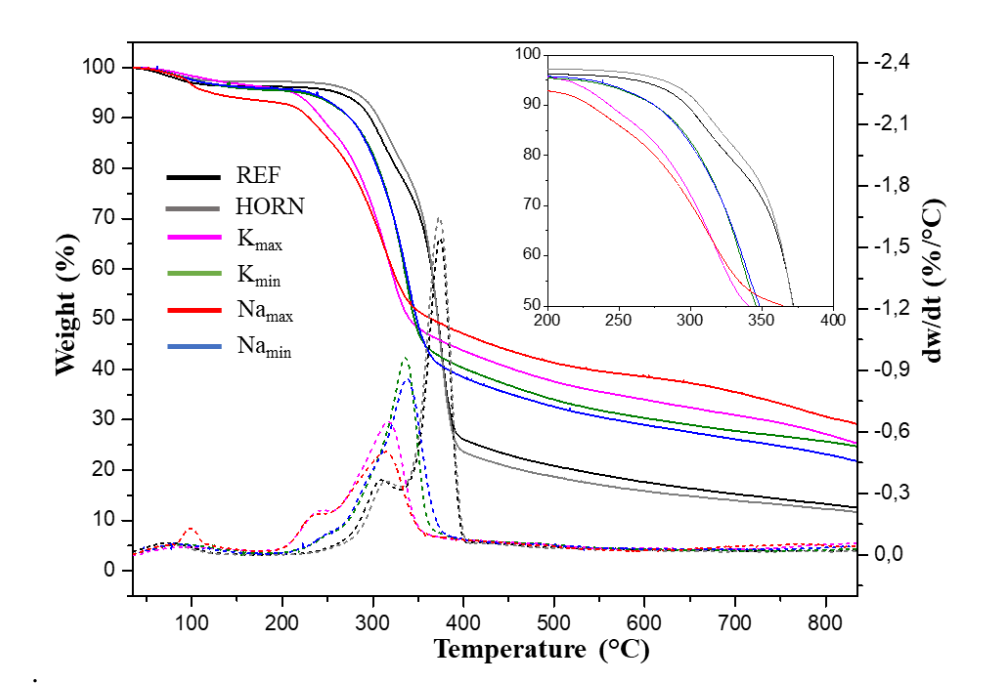


Figure 10 – Thermogravimetric analysis for fibers extracted from the matrix after exposure in 120Lab.

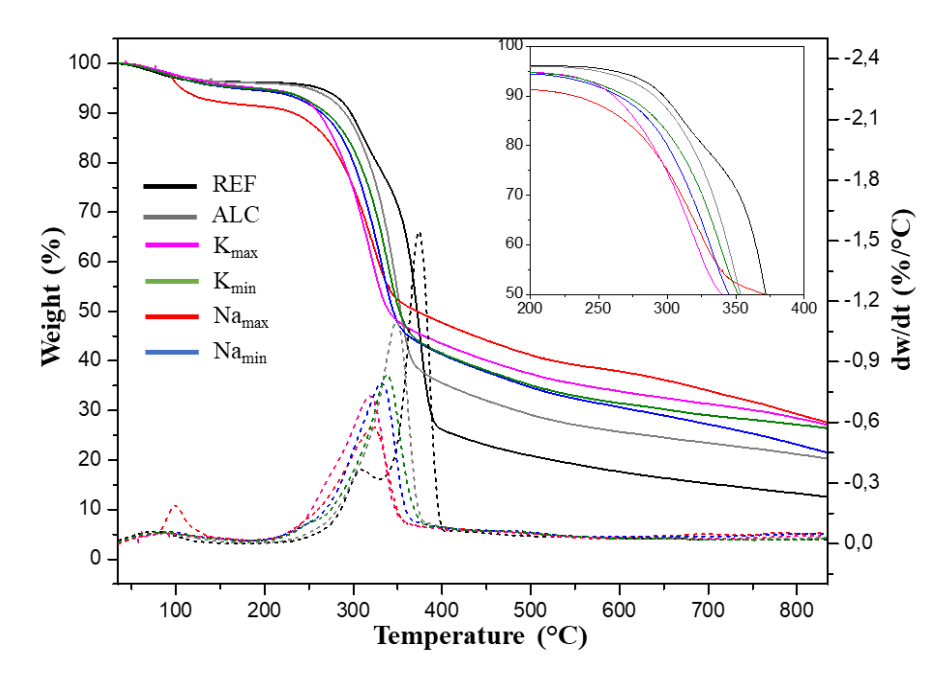


Figure 11 – Thermogravimetric analysis for fibers extracted from the matrix after exposure in 120Nat.

The fibers that were not incorporated into the matrix exhibited characteristic behavior (Fiore et al., 2016; Wei and Meyer, 2016), with a mass loss range between 258 °C and 353 °C, corresponding to hemicellulose decomposition, and between 332 °C and 404 °C, corresponding to cellulose decomposition. The reduced thermal stability of cellulose causes an overlap of peaks with hemicellulose in the DTG curve. However, it is worth noting that hemicellulose is easily decomposed in an alkaline environment, and no hemicellulose may be present in the fibers after exposure to different matrices. Fiore et al. (2016) observed a reduction in the hemicellulose peak after the alkaline treatment of vegetable fibers, which may have occurred after the fibers were exposed to the geopolymer matrices in this study. Additionally, Wei and Meyer (2016) demonstrated that cycles of wetting and drying also lead to hemicellulose decomposition and the disappearance of this peak in the DTG curve. This process occurred during the natural aging of the composites.

 With the aid of the curve referring to the first derivative of the mass variation (DTG), **Table 4** was obtained, with the values of the starting (T_i) , final (T_f) , and peak (T_p) temperatures of the thermal decomposition region of the cellulose.

Exposure	Temperature	Composites						
environments	(°C)	N_{\min}	N _{max}	K _{min}	K _{max}			
	$T_{\rm i}$	250.13	237.42	260.66	230.07			
28Lab	$\mathrm{T_{f}}$	356.27	354.27	366.30	353.60			
	T_p	329.69	324.55	338.39	314.48			
	$T_{\rm i}$	247.96	243.81	252.13	246.28			
120Lab	$\mathrm{T_{f}}$	359.11	355.94	356.77	352.99			
	T_p	331.87	326.02	331.03	321.89			
	T_{i}	272.86	261.33	268.85	268.01			
120Nat	$\mathrm{T_{f}}$	374.16	362.62	369.98	367.47			
	T_p	347.58	337.72	342.57	341.90			
	T_{i}	331.87						
REF (As received)	T_{f}	404.08						
(115 received)	T_p	374.16						

For all fibers extracted from the matrices, there was a reduction in the thermal decomposition temperature of cellulose compared to the reference fiber, indicating a decrease in the thermal stability of this component. This behavior was also noted by Zhou et al. (2014) during their study on alkaline treatment of vegetable fibers, highlighting that an alkaline environment lowers the thermal decomposition temperature of cellulose. Additionally, the thermal decomposition temperatures of cellulose were lower for fibers exposed in matrices with maximized free ions (Na_{max} and K_{max}), regardless of the exposure environment. Wei and Meyer (2016) emphasize that the reduction in the thermal decomposition temperature of cellulose may be caused by alkaline hydrolysis degradation of lignin and hemicellulose, which could have occurred more intensively in fibers exposed to Na_{max} and K_{max} .

Regarding lignin, the thermal decomposition of this component occurs across the entire temperature range studied, making it difficult to identify and quantify the influence of the matrix and aging environment on its decomposition.

3.5. Microstructural analysis by SEM

Figure 12 and Figure 13 present analyses of polished sections of the composites after aging in the laboratory and natural environment, respectively. Notably, all composites exhibit voids in the matrix-fiber interface zone, likely caused by the bending

test, where fibers were partially pulled out after the applied stress on the composite exceeded the fiber-matrix adhesion strength.

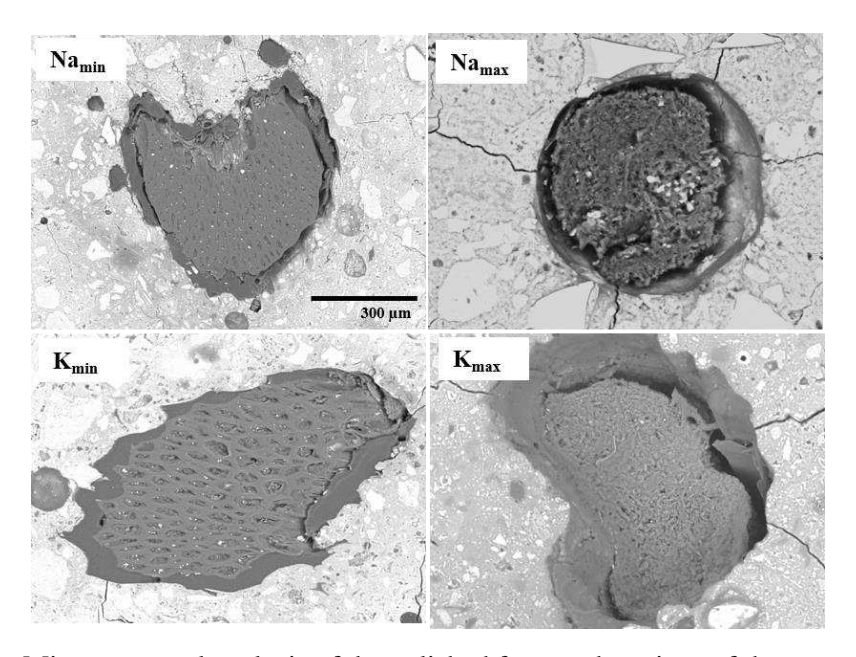


Figure 12 – Microstructural analysis of the polished fractured sections of the composites aged for 120 days in a laboratory environment.

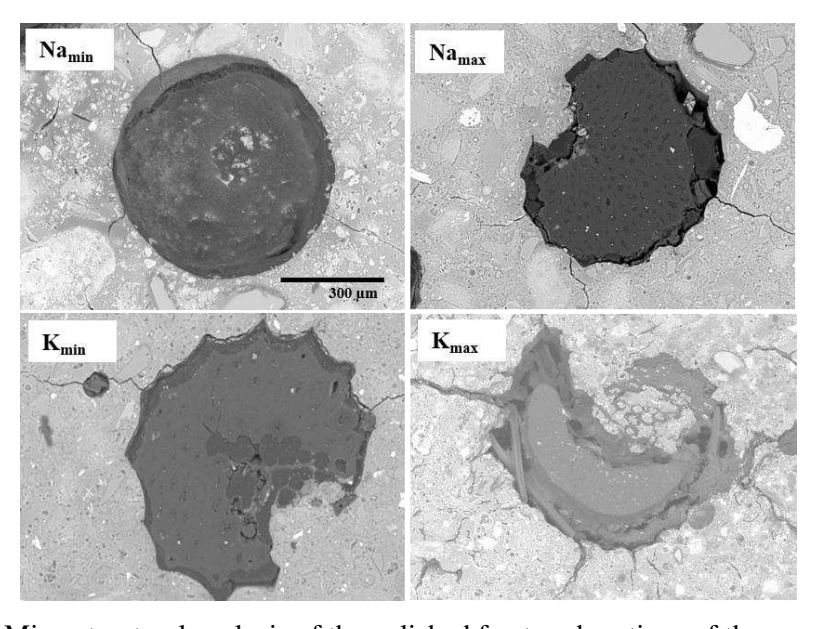


Figure 13 – Microstructural analysis of the polished fractured sections of the composites aged for 120 days in a natural environment.

The dimensions of the voids can be considered indicative of the intensity of fiber degradation. It is observed that the decomposition affects the outermost layers, primarily composed of amorphous and alkaline-sensitive components such as lignin and

hemicellulose. Wei and Meyer (2015) observed analogous behavior in analyses of fractured sections of Portland cement-based composites reinforced with vegetable fibers.

For both evaluated environments, it is noted that in composites produced with matrices optimized with maximized free alkaline ions (Na_{max} and K_{max}), the space between the matrix and the fiber is larger, likely due to the higher intensity of the alkaline hydrolysis process. Additionally, the results align with a three-point bending test conducted on the composite, where matrices dosed with minimized free alkaline ions (Na_{min} and K_{min}) did not exhibit significant toughness losses after composite aging.

It is also noteworthy that the fibers appear more intact for composites exposed to the natural environment and produced with Namin and Kmin matrices compared to composites exposed in the laboratory environment. While weathering in the natural environment can have adverse effects, causing dimensional variations in fibers and potentially enhancing void formation at the interface zone, it can also have positive effects by leaching free alkalis or promoting unintentional fiber hornification through observed wetting and drying cycles, as shown in **Figure 2**.

Figure 14 and Figure 15 present microstructural analyses of the fractured section of composites exposed in laboratory and natural environments, respectively. It is observed that fibers used as reinforcement in Na_{min} and K_{min} matrices maintain structural integrity, with few degradation points on their surface, likely caused by fiber pull-out during three-point bending test.

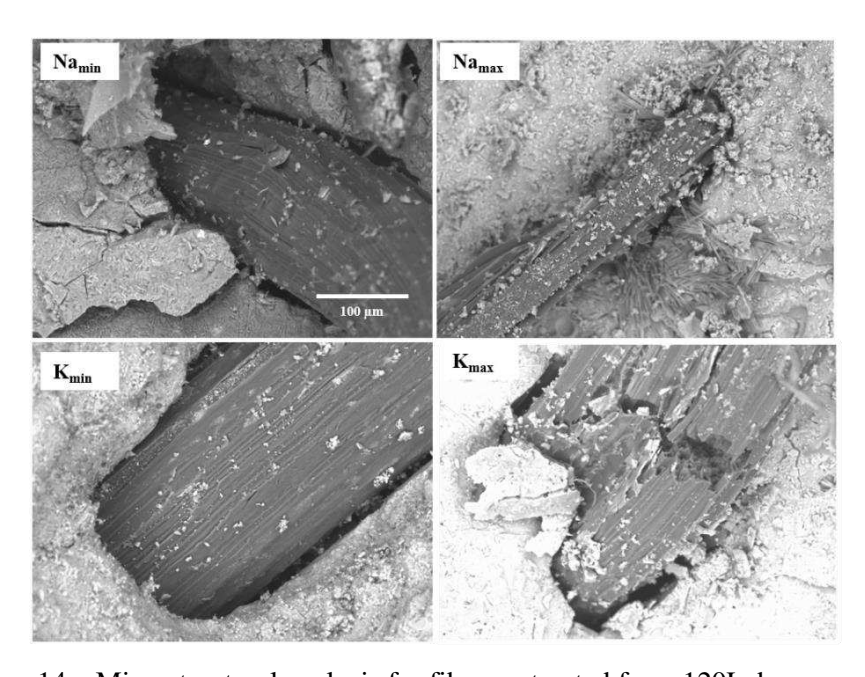


Figure 14 – Microstructural analysis for fibers extracted from 120Lab composites.

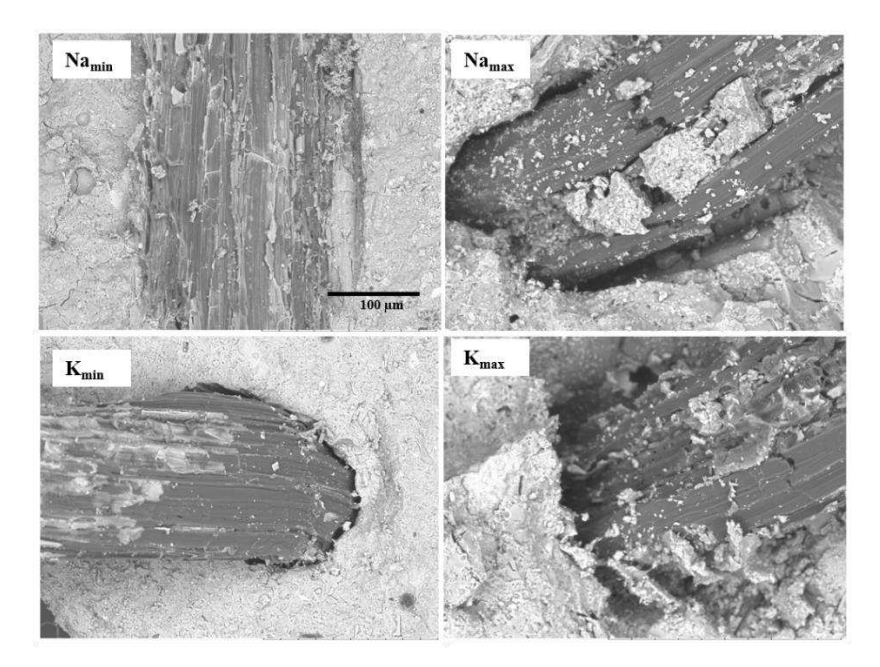


Figure 15 – Microstructural analysis for fibers extracted from 120Nat composites.

617 618

619

620

621

On the other hand, consistent with the previously evaluated properties, images of fibers in Na_{max} and K_{max} matrices depict an advanced process of surface degradation, with fractures indicating material fragility. The reduction in fiber tensile strength suggests that cellulose was also compromised; indeed, TG and FTIR analyses indicate chemical modifications in the fiber structure.

622623

624

625

626

627

628

629

630

631

632

633

634

635

636

3.6. Mechanisms and strategies to prevent fiber degradation

It is essential to revisit alkali-activation reactions to introduce the hypothesis of the degradation mechanism of vegetable fibers in an alkaline matrix and propose a plausible solution based on dosing mechanisms. According to Glukhovsky's conceptual model (1959), these reactions occur in three main stages: dissolution-coagulation, coagulation-condensation, and condensation-crystallization. Initially, reactive aluminosilicates are rapidly dissolved by OH anions from the activating solution, releasing tetrahedral units of [SiO₄] and [AlO₄]. These units polymerize by sharing oxygen atoms, forming Si-O-Al-O bonds. The resulting gel (condensation) forms threedimensional structures through hydrogen bonding. Simultaneously, the negative charge of Al is balanced by cations such as Na⁺ and K⁺. In a hypothetical scenario where all alumina in the precursor is reactive, the ideal molar ratio of (Na₂O or K₂O)/Al₂O₃ to avoid free alkaline cations would be 1. Excess of this ratio results in free alkaline ions in the

matrix pore solution, while excess OH⁻ anions also influence the degradation of vegetable fibers.

Based on consolidated geopolymerization models (Glukhovsky 1959; Lolli et al., 2018), the fiber degradation mechanisms detailed by Wei and Meyer (2015), and the theory of sodium cellulose formation presented by Klemm et al. (1998), **Figure 16** describes the likely mechanism of degradation of vegetable fibers exposed to alkaline binders. This mechanism aligns with the results observed in thermogravimetric analysis, where fibers extracted from the matrix were found to be less stable than reference fibers, likely due to the formation of a new structure that is more easily thermally decomposed. Chemical modifications in the fiber structure were also observed in FTIR analysis, possibly caused by the actions of free alkaline ions in the matrix.

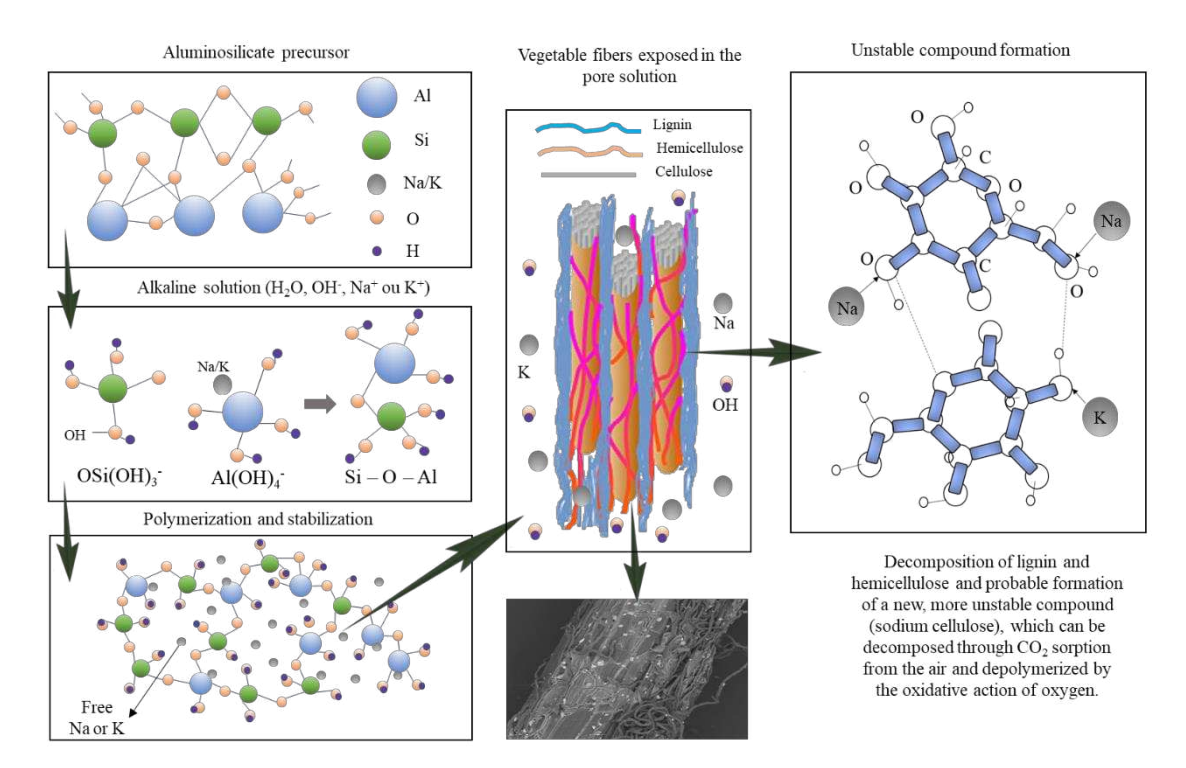


Figure 16 – Description of the probable degradation mechanism of vegetable fibers in alkaliactivated binders.

As evidenced in all evaluated properties, the degradation of fibers extracted from composites with minimized free alkaline ions (Na_{min} and K_{min}) was less intense than fibers produced with matrices having maximized free alkaline ions (Na_{max} and K_{max}). In this regard, plausible solutions to prevent fiber degradation are associated with optimizing the (Na_2O or K_2O)/ Al_2O_3 ratio close to 1, ensuring fixation of free alkalis, and using precursors with higher purity, contributing to fixing Na^+ or K^+ ions. As for OH^- ions,

these are incorporated into the mixtures through alkali hydroxide (NaOH or KOH), and although crucial for precursor dilution, they are directly controlled by the proportion of sodium or potassium in the binder dosing. Minimizing or maximizing these elements directly affects the minimization or maximization of available hydroxyl ion concentrations in the composite pore water.

4. CONCLUSIONS

To evaluate the durability of vegetable fibers as reinforcement in geopolymeric matrices, composites were produced with matrices of varying concentrations and alkaline bases exposed to natural and laboratory environments. Based on the analysis of the results, it was observed that:

According to the FTIR analysis, both activating solutions resulted in a gradual reduction of the bands associated with lignin, hemicellulose, and cellulose, which aligns with the mechanism of alkaline hydrolysis.

The natural exposure environment caused increased water absorption in Na_{max} and K_{max} composites, indicating fiber decomposition and leaching in highly alkaline environments or matrix leaching due to environmental weathering cycles of wetting and drying. Load-deflection curve analysis showed that vegetable fibers provide ductile behavior in geopolymeric binders, with energy absorption after the first crack.

Regarding the LOP, it was observed that the natural exposure environment also negatively affects this property, primarily governed by the tensile strength of the matrix. However, vegetable fibers can maintain and increase the composite's strength, provided that the alkalinity of the matrix does not compromise its chemical and physical stability, as observed in the specific energy analysis, where higher values were obtained for composites produced with matrices optimized with minimized free ions.

Overall, composites produced with the K_{min} matrix could recover and increase the load supported after the first crack, indicating that in this matrix, regardless of the environment and exposure time, fiber degradation did not compromise its ability to act as an anchoring element for the matrix. Regarding fiber-matrix adhesion, the K_{min} matrix appears to be the least severe environment for vegetable fibers.

The thermogravimetric analysis also corroborates the FTIR results and the mechanical analyses, which showed a disappearance of the hemicellulose decomposition peaks and a reduction in the temperature at which cellulose begins its thermal

decomposition. The microstructural analysis depicts voids at the interface zone and highlights the degradation process observed in fibers exposed to Na_{max} and K_{max} .

Through the combined analysis of the results, it is plausible that after lignin and hemicellulose degradation, reactions occur between cellulose and free alkaline ions (Na or K), forming a less stable and less resistant compound. These results differ from several previously published works that point to vegetable fibers as a solution for the brittle behavior of geopolymeric binders. However, it has been shown here that controlling matrix aggressiveness is a viable approach to enable the association of these two materials. A formulation with higher efficiency in fixing free ions and optimizing the Na₂O/Al₂O₃ ratio will likely yield better results.

702

692 693

694

695

696

697

698

699

700

701

703704

ACKNOWLEDGMENTS

705 The authors would like to acknowledge the financial support of CNPq (Process n°

309270/2022-7), FAPESB (Process n° 0486/2020) and CAPES (Process n°

707 88887.838290/2023-00).

708

709

706

DECLARATION OF COMPETING INTEREST

The authors declare that they have no known competing financial interests or personal relationships that could have appeared to influence the work reported in this paper.

713

714

REFERÊNCIAS

- 715 J. L. Provis, S.A. Bernal. Geopolymers and related alkali-activated materials. **Annu. Rev.**
- 716 **Mater. Res.**, v. 44, p. 299-327, 2014. https://doi.org/10.1146/annurev-matsci-070813-
- 717 113515
- 718 A. Mohajerani, D. Suter, T. Jeffrey-Bailey, T. Song, A. Arulrajah, S. Horpibulsuk, D.
- 719 Law. Recycling waste materials in geopolymer concrete. Clean Technol. Environ.
- **Policy**, v. 21, n. 3, p. 493-515, 2019. https://doi.org/10.1007/s10098-018-01660-2
- H. A. Santana, J. S. Andrade Neto, N. S. Amorim Júnior, D. V. Ribeiro, M. S. Cilla, C.
- M. Dias. Self-compacting geopolymer mixture: Dosing based on statistical mixture
- design and simultaneous optimization. **Construction and Building Materials**, v. 249, p.
- 724 118677, 2020. https://doi.org/10.1016/j.conbuildmat.2020.118677

- B. Singh, G. Ishwarya, M. Gupta, S. K. Bhattacharyya. Geopolymer concrete: A review
- of some recent developments. **Construction and Building Materials**, v. 85, p. 78-90,
- 727 2015. https://doi.org/10.1016/j.conbuildmat.2015.03.036
- 728 M. Alzeer, K.Mackenzie. Synthesis and mechanical properties of novel composites of
- 729 inorganic polymers (geopolymers) with unidirectional natural flax fibres (phormium
- 730 tenax). **Applied Clay Science**, v. 75, p. 148-152, 2013.
- 731 <u>https://doi.org/10.1016/j.clay.2013.03.010</u>
- L. Yan, B. Kasal, L. Huang. A review of recent research on the use of cellulosic fibres,
- 733 their fibre fabric reinforced cementitious, geo-polymer and polymer composites in civil
- engineering. Composites Part B: Engineering, v. 92, p. 94-132, 2016.
- 735 <u>https://doi.org/10.1016/j.compositesb.2016.02.002</u>
- 736 K. Korniejenko, E. Fraczek, E. Pytlak, M. Adamski. Mechanical properties of
- geopolymer composites reinforced with natural fibers. **Procedia Engineering**, v. 151, p.
- 738 388-393, 2016. https://doi.org/10.1016/j.proeng.2016.07.395
- G. H. D. Tonoli, U. P. Rodrigues Filho, Jr, H. Savastano, J. Bras, M. N. Belgacem, F. R.
- 740 Lahr. Cellulose modified fibres in cement based composites. Composites Part A:
- 741 Applied Science and Manufacturing, v. 40, n. 12, p. 2046-2053, 2009.
- 742 <u>https://doi.org/10.1016/j.compositesa.2009.09.016</u>
- G. Lazorenko, A. Kasprzhitskii, A. Kruglikov, V. Mischinenko, V. Yavna. Sustainable
- 744 geopolymer composites reinforced with flax tows. Ceramics International, 2020.
- 745 <u>https://doi.org/10.1016/j.ceramint.2020.01.184</u>
- H. Assaedi, F. U. A. Shaikh, I. M. Low. Effect of nanoclay on durability and mechanical
- 747 properties of flax fabric reinforced geopolymer composites. **Journal of Asian Ceramic**
- **Societies**, v. 5, n. 1, p. 62-70, 2017. https://doi.org/10.1016/j.jascer.2017.01.003
- 749 T. Alomayri, F. U. A. Shaikh, I. M, Low. Thermal and mechanical properties of cotton
- fabric-reinforced geopolymer composites. **Journal of materials science**, v. 48, n. 19, p.
- 751 6746-6752, 2013. https://doi.org/10.1007/s10853-013-7479-2
- E. A. S. Correia, S. M. Torres, M. E. Oliveira Alexandre, K. C. Gomes, N. P. Barbosa, S.
- 753 R. Barros. Mechanical performance of natural fibers reinforced geopolymer composites.
- 754 In: Materials Science Forum. Trans Tech Publications Ltd, 2013. p. 139-145.
- 755 https://doi.org/10.4028/www.scientific.net/MSF.758.139
- 756 L. C. Alves, R. A. Ferreira, L. B. Machado, L. A. Motta. Optimization of metakaolin-
- 757 based geopolymer reinforced with sisal fibers using response surface methology.
- 758 **Industrial Crops and Products**, v. 139, p. 111551, 2019.
- 759 https://doi.org/10.1016/j.indcrop.2019.111551
- A. Wongsa, R. Kunthawatwong, S. Naenudon, V. Sata, P. Chindaprasirt. Natural fiber
- 761 reinforced high calcium fly ash geopolymer mortar. Construction and Building
- 762 **Materials**, v. 241, p. 118143, 2020. https://doi.org/10.1016/j.conbuildmat.2020.118143
- 763 K. Siddharth, D. Dinakar, V. Suresh, C. Balaji, M. D. Kumar. Strength Studies on Silica
- Fume Based Geopolymer Mortar with Coir Fibre, International Research Journal of
- **Engineering and Technology**, Vol. 3(12), pp. 359-363, 2016.
- 766 F. Amalia, N. Akifah. Development of Coconut Trunk Fiber Geopolymer Hybrid
- 767 Composite for Structural Engineering Materials. In: **IOP Conference Series: Materials**
- 768 Science and Engineering. IOP Publishing, p. 012014, 2017. https://
- 769 <u>doi.org/10.1088/1757-899X/180/1/012014</u>

- 770 R. D. Toledo Filho, F. A. Silva, E. M. R. Fairbairn, J. A. Melo Filho. Durability of
- 771 compression molded sisal fiber reinforced mortar laminates. Construction and building
- 772 **materials**, v. 23, n. 6, p. 2409-2420, 2009.
- 773 <u>https://doi.org/10.1016/j.conbuildmat.2008.10.012</u>
- 774 M. M. Kabir, H. Wang, K. T. Lau, F. Cardonam. Chemical treatments on plant-based
- natural fibre reinforced polymer composites: **An overview. Composites: Part B**, v. 43,
- pg. 2883-2892, 2012. https://doi.org/10.1016/j.compositesb.2012.04.053
- E. Gallucci, K. Scrivener. Crystallisation of calcium hydroxide in early age model and
- ordinary cementitious systems. **Cement and Concrete Research**, v. 37, n. 4, p. 492-501,
- 779 2007. https://doi.org/10.1016/j.cemconres.2007.01.001
- 780 LIMA, P. R. L.; TOLEDO FILHO, R. D. Use of metakaolin to improve the durability of
- sisal fiber-cement based composites. **Ambiente Construído**, v. 8, n. 4, p. 7-19, 2008.
- 782 LIMA, P. R.; SANTOS, R. J.; FERREIRA, S. R.; TOLEDO FILHO, R. D.
- 783 Characterization and treatment of sisal fiber residues for cement-based composite
- 784 application. **Engenharia Agrícola**, v. 34, p. 812-825, 2014.
- PIZZOL, V. D.; MENDES, L. M.; FREZZATTI, L.; SAVASTANO JR, H.; TONOLI, G.
- 786 H. D. Effect of accelerated carbonation on the microstructure and physical properties of
- hybrid fiber-cement composites. **Minerals Engineering**, v. 59, p. 101-106, 2014.
- 788 ALMEIDA, A. E. F. D. S.; TONOLI, G. H. D.; SANTOS, S. F. D.; SAVASTANO JR,
- 789 H. Improved durability of vegetable fiber reinforced cement composite subject to
- accelerated carbonation at early age. Cement and Concrete Composites, v. 42, p. 49-
- 791 58, 2013.
- 792 M. Romagnoli, P. Sassatelli, M. Lassinantti Gualtieri, G. Tari, Rheological
- characterization of fly ash-based suspensions, **Constr. Build. Mater**. 65 (2014) 526–534.
- 794 https://doi.org/10.1016/J.CONBUILDMAT.2014.04.130.
- Latella, B. A., Perera, D. S., Durce, D., Mehrtens, E. G., & Davis, J. (2008). Mechanical
- properties of metakaolin-based geopolymers with molar ratios of Si/Al \approx 2 and Na/Al \approx 1.
- **Journal of materials science**, 43, 2693-2699.
- 798 Alonso, M. M., Gismera, S., Blanco, M. T., Lanzón, M., & Puertas, F. Alkali-activated
- 799 mortars: Workability and rheological behaviour. **Construction and Building Materials**,
- 800 v. 145, p. 576-587, 2017.
- 801 DIAS, Cleber Marcos Ribeiro; SAVASTANO JR, HOLMER; JOHN, Vanderley Moacyr.
- Functionally graded fiber-cement: extrudable mixtures for gradation of hatschek-made
- so corrugated sheets. **Proceedings IIBCC**, 2018.
- FERREIRA, Saulo Rocha et al. Effect of fiber treatments on the sisal fiber properties and
- fiber-matrix bond in cement based systems. Construction and Building Materials, v.
- 806 101, p. 730-740, 2015.
- FERREIRA, Saulo Rocha et al. Effect of hornification on the structure, tensile behavior
- and fiber matrix bond of sisal, jute and curauá fiber cement based composite
- systems. **Construction and Building Materials**, v. 139, p. 551-561, 2017.
- Page, J., Khadraoui, F., Gomina, M., & Boutouil, M. (2019). Influence of different surface
- treatments on the water absorption capacity of flax fibres: Rheology of fresh reinforced-
- mortars and mechanical properties in the hardened state. Construction and Building
- 813 **Materials**, 199, 424-434.

- Juárez, C., Guevara, B., Valdez, P., & Durán-Herrera, A. (2010). Mechanical properties
- of natural fibers reinforced sustainable masonry. Construction and Building
- Materials, 24(8), 1536-1541. https://doi.org/10.1016/j.buildenv.2005.12.005
- 817 KANI, Ebrahim Najafi; ALLAHVERDI, Ali; PROVIS, John L. Efflorescence control in
- geopolymer binders based on natural pozzolan. Cement and Concrete Composites, v.
- 34, n. 1, p. 25-33, 2012. https://doi.org/10.1016/J.CEMCONCOMP.2011.07.007
- DE ALMEIDA MELO FILHO, João; DE ANDRADE SILVA, Flávio; TOLEDO FILHO,
- 821 Romildo Dias. Degradation kinetics and aging mechanisms on sisal fiber cement
- composite systems. Cement and Concrete Composites, v. 40, p. 30-39, 2013.
- BENTUR, Arnon; MINDESS, Sidney. Fibre reinforced cementitious composites. Crc
- 824 Press, 2006.
- FERREIRA, Saulo Rocha et al. The influence of carboxylated styrene butadiene rubber
- 826 coating on the mechanical performance of vegetable fibers and on their interface with a
- cement matrix. Construction and Building Materials, v. 262, p. 120770, 2020.
- Júnior, N. S. A., Neto, J. S. A., Santana, H. A., Cilla, M. S., & Ribeiro, D. V. Durability
- and service life analysis of metakaolin-based geopolymer concretes with respect to
- chloride penetration using chloride migration test and corrosion potential. Construction
- **and Building Materials**, v. 287, p. 122970, 2021.
- WEI, Jianqiang; MEYER, Christian. Degradation mechanisms of natural fiber in the
- matrix of cement composites. **Cement and concrete Research**, v. 73, p. 1-16, 2015.
- Zhang, B., Zhu, H., Feng, P. e Zhang, P. A review on shrinkage-reducing methods and
- 835 mechanisms of alkali-activated/geopolymer systems: Effects of chemical
- additives. **Journal of Building Engineering**, v. 49, p. 104056, 2022.
- 837 Santana, H. A., Júnior, N. S. A., Ribeiro, D. V., Cilla, M. S., & Dias, C. M. Vegetable
- 838 fibers behavior in geopolymers and alkali-activated cement based matrices: A
- review. **Journal of Building Engineering**, v. 44, p. 103291, 2021.
- 840 BALLESTEROS, Julian Eduardo Mejia et al. Synergic effect of fiber and matrix
- treatments for vegetable fiber reinforced cement of improved performance. Construction
- and Building Materials, v. 205, p. 52-60, 2019.
- 843 Gram HE. Natural fibre concrete roofing. Concrete technology and design, vol. 5: natural
- fibre reinforced cement and concrete. London: Blackie and Son Ltd.; 1988. p. 256–84.
- 845 EL OUDIANI, Asma; MSAHLI, Slah; SAKLI, Faouzi. In-depth study of agave fiber
- structure using Fourier transform infrared spectroscopy. Carbohydrate polymers, v.
- 847 164, p. 242-248, 2017.
- 848 ZHOU, Feng; CHENG, Guangxu; JIANG, Bo. Effect of silane treatment on
- microstructure of sisal fibers. **Applied Surface Science**, v. 292, p. 806-812, 2014.
- 850 KAMARUDIN, Siti Hasnah et al. Thermal and structural analysis of epoxidized jatropha
- 851 oil and alkaline treated kenaf fiber reinforced poly (Lactic acid)
- biocomposites. **Polymers**, v. 12, n. 11, p. 2604, 2020.
- MOHAN, T. P.; KANNY, Krishnan. Chemical treatment of sisal fiber using alkali and
- clay method. Composites Part A: Applied Science and Manufacturing, v. 43, n. 11, p.
- 855 1989-1998, 2012.

- 856 FIORE, V. et al. A new eco-friendly chemical treatment of natural fibres: Effect of
- sodium bicarbonate on properties of sisal fibre and its epoxy composites. Composites
- 858 **Part B: Engineering**, v. 85, p. 150-160, 2016.
- 859 FIORE, V. et al. A new eco-friendly chemical treatment of natural fibres: Effect of
- sodium bicarbonate on properties of sisal fibre and its epoxy composites. Composites
- **Part B: Engineering**, v. 85, p. 150-160, 2016.
- 862 ZHOU, Feng; CHENG, Guangxu; JIANG, Bo. Effect of silane treatment on
- microstructure of sisal fibers. **Applied Surface Science**, v. 292, p. 806-812, 2014.
- Marvila, M. T., Rocha, H. A., de Azevedo, A. R. G., Colorado, H. A., Zapata, J. F., &
- Vieira, C. M. F. Use of natural vegetable fibers in cementitious composites: Concepts and
- applications. **Innovative Infrastructure Solutions**, v. 6, p. 1-24, 2021.
- ASTM C1557, Standard Test Method for Tensile Strength and Young's Modulus of
- 868 Fibers. West Conshohocken, PA, USA: American Society for Testing and Materials;
- 869 2008.
- Santana, H. A., Júnior, N. S. A., Carneiro, G. O., Ribeiro, D. V., Cilla, M. S., & Dias, C.
- 871 M. Asbestos-cement wastes as supplementary precursors of NaOH-activated
- binders. Construction and Building Materials, v. 364, p. 129921, 2023.
- Dias, C. M. R., Cincotto, M. A., Savastano Jr, H., & John, V. M. Long-term aging of
- 874 fiber-cement corrugated sheets-The effect of carbonation, leaching and acid
- rain. Cement and Concrete Composites, v. 30, n. 4, p. 255-265, 2008.
- 876 Lolli, F., Manzano, H., Provis, J. L., Bignozzi, M. C., & Masoero, E. (2018). Atomistic
- 877 simulations of geopolymer models: the impact of disorder on structure and
- mechanics. **ACS applied materials & interfaces**, 10(26), 22809-22820.
- Javier-Astete, R.; Jimenez-Davalos, J.; Zolla, G. Determination of hemicellulose,
- 880 cellulose, holocellulose and lignin content using FTIR in Calycophyllum spruceanum
- 881 (Benth.) K. Schum. and Guazuma crinita Lam. PLoS One, v. 16, n. 10, p. e0256559, 2021.
- 882 SALIM, R.; ASIK, J.; SARJADI, M. S. Chemical functional groups of extractives,
- cellulose and lignin extracted from native Leucaena leucocephala bark. Wood Science
- and Technology, v. 55, p. 295-313, 2021.
- 885 El Oudiani, A.; Msahli, S.; Sakli, F. In-depth study of agave fiber structure using Fourier
- transform infrared spectroscopy. Carbohydrate polymers, v. 164, p. 242-248, 2017.
- Yang, H., Yan, R., Chen, H., Lee, D. H., & Zheng, C. Characteristics of hemicellulose,
- cellulose and lignin pyrolysis. **Fuel**, v. 86, n. 12-13, p. 1781-1788, 2007.
- 889 Santana, H. A., Andrade Neto, J. S., Ribeiro, D. V., Cilla, M. S., Dias, C. M. Accelerated
- alkaline attack of 3D printing polymers to assess their durability in geopolymer-based
- matrices. Journal of Materials in Civil Engineering, v. 33, n. 11, p. 04021327, 2021.